RESEARCH ARTICLE

Multiple Slip Mechanism for Converging/Diverging Flow of Second Grade Nanofluids with Thermal Performance

Hashim[1,*] **and Akhunzadi Laiba Iftikhar**[1]

[1] Department of Mathematics and Statistics, University of Haripur, Haripur 22620, Pakistan

Abstract

This study presents a comprehensive numerical investigation of the flow and heat transfer characteristics of a second-grade nanofluid in a converging/diverging channel, incorporating the significant effects of multiple slip mechanisms. The analysis considers velocity, thermal, and solutal slip conditions at the channel walls, providing a more realistic model of nanofluid behavior in micro-environments or with specific surface interactions. The governing equations, derived from the principles of conservation of mass, momentum, and energy, are formulated using a non-Newtonian second-grade fluid model to account for viscoelastic effects, combined with the Buongiorno model to capture the Brownian motion and thermophoresis mechanisms of nanoparticles. The resulting system of highly non-linear, coupled partial differential equations is transformed into a set of ordinary differential equations using a similarity transformation approach. The ensuing boundary value problem is solved computationally using the robust MATLAB bvp4c solver. The results are meticulously analyzed to elucidate the intertwined influence of the second-grade fluid parameter (viscoelasticity), the nanoparticle volume fraction, the slip parameters, and the channel geometry (converging/diverging angle) on the velocity profile, temperature distribution, and thermal performance. Key findings indicate that velocity slip and thermal slip parameters substantially reduce skin friction and enhance the local Nusselt number, respectively, thereby critically optimizing the thermal performance of the system. Furthermore, the converging channel geometry is shown to synergize with the viscoelastic nature of the second-grade fluid to significantly augment heat transfer rates compared to the diverging case.

Keywords: second grade nanofluid, converging/diverging channel, multiple slip, heat transfer enhancement, viscoelastic fluid, numerical solution.

1 Introduction

It has been well-known that the demand for working fluids in thermal processes is increasing day by day due to their energy release to the system. However, working fluids like oil, water and other similar

Submitted: 01 September 2025
Accepted: 02 October 2025
Published: 25 November 2025

Vol. 1, **No.** 2, 2025.
10.62762/IJTSSE.2025.412468

***Corresponding author:**
✉ Hashim
hashim@uoh.edu.pk

Citation
Hashim, & Iftikhar, A. L. (2025). Multiple Slip Mechanism for Converging/Diverging Flow of Second Grade Nanofluids with Thermal Performance. *International Journal of Thermo-Fluid Systems and Sustainable Energy*, 1(2), 64–74.

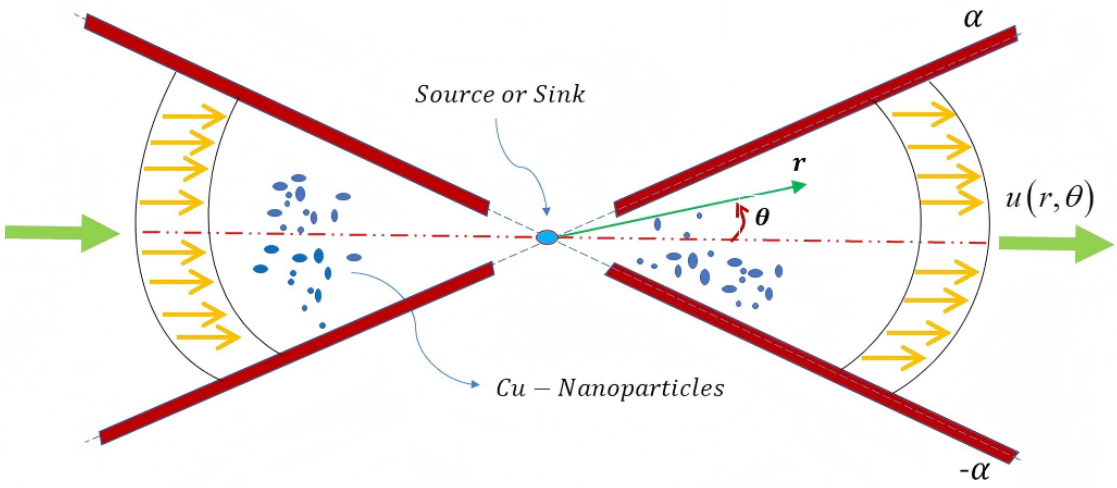

Figure 1. Schematic diagram of the converging/diverging channel flow with multiple slip mechanisms.

fluids may be identified owing to their low thermal properties vulnerable to the limitations of their energy transport performance. To ameliorate the energy transport properties of thermal liquids, which is to enhance the rate of heat trans- mission by virtue of their higher thermic conductivity than the working liquids. In the ongoing search for new techniques to improve heat transmission, metallic nanoparticles with higher thermal conductivity were added to common working liquids by Choi et al. [1], who called them nanofluids (NFs). The improved performance of nanofluids compared to working fluids, confirmed by both computational and experimental investigations, has propelled the researchers to explore this field of science in recent decades. Several disciplines of heat transfer have used nanofluids, including electronic devices, food industry, biomedicine, liquid metal cooling, drug delivery, solar panels, nuclear re- actors, etc. The two-phase model, first proposed by Buongiorno [2], is one of the typical methods used for heat transmission in nanofluids. He looked at the slip mechanism and considered the solid and fluid as interpenetrating continua, each moving at its own speed but with slip velocity. Later, Khan et al. [3] introduced the innovative idea of laminar flow involving nanofluids driven by a stretching surface. Makinde et al. [4] extended this work by incorporating the effect of convective heat transport for nanofluid flow past a stretching surface. There is a substantial quantity of literature on nanofluid in recent advancements, for both Newtonian and non-Newtonian models, however we only include a few current works [5–10].

The no-slip condition at the boundary was a problem that was taken into consideration in the early stages of fluid mechanics, and various experiments supported its validity. The no-slip boundary criterion is simply a model based on empirical data. Moreover, nonslip boundary conditions are invalid in several physical situations, including low-pressure flows and flows at the micro- and nanoscale. Similarly, hydrophobicity and roughness of the wall, which alter the hydrodynamic conditions at the surface, may be the cause of the slip at the wall. The wide-spread applications of slip condition at the surface contain polishing artificial heart valves, microfluidic devices, lubrications, biological fluids, flow of non-Newtonian fluids in industry, etc. The contact-line singularity that would normally restrict the movement of a half-submerged sphere normal to a planner free surface enclosing a semi-infinite viscous fluid was eliminated by O'Neill et al. [11] using a linear slip boundary condition. Numerous studies in recent years have revealed that fluid slippage may occur at the surface of solid boundaries. For instance, Nadeem et al. [12] explored the flow of non-Newtonian fourth grade fluid subject to partial slip conditions at the boundary. Later, Ashmawy [13] employed a linear slip condition to investigate time-dependent Couette flow of micropolar fluid through a channel. Devakar et al. [14] presented the analytical solution for couple stress fluid flow by using velocity slip conditions. Hayat et al. [15] examined the impacts of inclined magnetic field and partial slip-on peristaltic flow tangent hyperbolic nanofluids through inclined

channel. Khan et al. [16] computed multiple numerical solutions for slip flow of nanofluids with thermal radiation impacts. Few recent studies on these aspects can be found in [17–22].

2 Problem Formulation

The present work deals with the incompressible, two-dimensional flow of a second-grade fluid flowing between two inclined nonparallel walls that are at an angle of 2α. A source or sink at the intersection of two non-parallel walls causes the flow to occur. About the centerlines $\theta = 0$, the symmetric character of flow is considered. The radial direction is set parallel and axial direction perpendicular to the flow. Slip boundary conditions are taken on the channel walls. The schematic diagram of the physical problem is depicted in Figure 1.

The basic governing equations (continuity, momentum, energy & concentration) using Buongiorno's model of nanofluids are given below:

Mass balance equation:

$$\rho_f \left(\frac{\partial}{\partial r}(ru)\right) = 0. \tag{1}$$

Momentum balance equations:

r - component:

$$\begin{aligned} u\frac{\partial u}{\partial r} =& -\frac{1}{\rho_f}\frac{\partial p}{\partial r} + v_f\left(2\frac{\partial^2 u}{\partial r^2} + \frac{2}{r}\frac{\partial u}{\partial r} + \frac{1}{r^2}\frac{\partial^2 u}{\partial \theta^2} - \frac{2u}{r^2}\right) \\ &+ \frac{a_1}{\rho}\left[\frac{2u}{r^2}\frac{\partial^2 u}{\partial r^2} + 2\frac{\partial u}{\partial r}\frac{\partial^2 u}{\partial r^2} - \frac{2}{r^3}\left(\frac{\partial u}{\partial \theta}\right)^2\right. \\ &\left.+2u\frac{\partial^3 u}{\partial r^3} - \frac{1}{r^2}\frac{\partial u}{\partial \theta}\frac{\partial^2 u}{\partial r \partial \theta}\right] \\ &+ \frac{a_1}{\rho}\left[\frac{1}{r^2}\frac{\partial u}{\partial \theta}\frac{\partial^2 u}{\partial r \partial \theta} + \frac{1}{r^2}\frac{\partial u}{\partial r}\frac{\partial^2 u}{\partial \theta^2} + \frac{u}{r^2}\frac{\partial^3 u}{\partial r \partial \theta^2}\right. \\ &\left.+\frac{2u^2}{r^3} - \frac{2u}{r^2}\frac{\partial u}{\partial r} - \frac{2u}{r^3}\frac{\partial^2 u}{\partial \theta^2}\right]. \end{aligned} \tag{2}$$

θ - component:

$$\begin{aligned} 0 =& -\frac{1}{r\rho_f}\frac{\partial p}{\partial \theta} + v_f\left(\frac{1}{r}\frac{\partial^2 u}{\partial r \partial \theta} + \frac{3}{r^2}\frac{\partial u}{\partial \theta}\right) \\ &+ \frac{a_1}{\rho}\left[\frac{u}{r^2}\frac{\partial^2 u}{\partial r \partial \theta} + \frac{1}{r^2}\frac{\partial u}{\partial r}\frac{\partial u}{\partial \theta} + \frac{1}{r}\frac{\partial u}{\partial \theta}\frac{\partial^2 u}{\partial r^2}\right. \\ &+\frac{2}{r}\frac{\partial u}{\partial r}\frac{\partial^2 u}{\partial r \partial \theta} + \frac{u}{r}\frac{\partial^3 u}{\partial r^2 \partial \theta} \\ &\left.+\frac{2}{r^3}\frac{\partial u}{\partial \theta}\frac{\partial^2 u}{\partial \theta^2} - \frac{4u}{r^3}\frac{\partial u}{\partial \theta}\right]. \end{aligned} \tag{3}$$

Energy balance equation:

$$\begin{aligned} (\rho c_p)\frac{u}{\partial r}\frac{\partial T}{\partial r} =& k_f\left[\frac{\partial^2 T}{\partial r^2} + \frac{1}{r}\frac{\partial T}{\partial r} + \frac{1}{r^2}\frac{\partial^2 T}{\partial \theta^2}\right] \\ &+ \mu\left(4\left(\frac{\partial u}{\partial r}\right)^2 + \frac{1}{r^2}\left(\frac{\partial u}{\partial \theta}\right)^2\right) \\ &+ \alpha_1\left[2u\frac{\partial^2 u}{\partial r^2}\frac{\partial u}{\partial r} + \frac{u}{r^2}\frac{\partial u}{\partial \theta}\frac{\partial^2 u}{\partial r \partial \theta}\right. \\ &\left.+\frac{4u^2}{r^2}\frac{\partial u}{\partial r} - \frac{u}{r^3}\left(\frac{\partial u}{\partial \theta}\right)^2\right] \\ &+ (\rho c_p)_s\left(D_B\left[\frac{\partial T}{\partial r}\frac{\partial C}{\partial r} + \frac{1}{r^2}\frac{\partial T}{\partial \theta}\frac{\partial C}{\partial \theta}\right]\right. \\ &\left.+\frac{D_T}{T_0}\left[\left(\frac{\partial T}{\partial r}\right)^2 + \frac{1}{r^2}\left(\frac{\partial T}{\partial \theta}\right)^2\right]\right). \end{aligned} \tag{4}$$

Concentration balance equation:

$$\begin{aligned} U_r\frac{\partial C}{\partial r} =& D_B\left(\frac{\partial^2 C}{\partial r^2} + \frac{1}{r}\frac{\partial C}{\partial r} + \frac{1}{r^2}\frac{\partial^2 C}{\partial \theta^2}\right) \\ &+ \frac{D_T}{T_0}\left(\frac{\partial^2 T}{\partial r^2} + \frac{1}{r}\frac{\partial T}{\partial r} + \frac{1}{r^2}\frac{\partial^2 T}{\partial \theta^2}\right). \end{aligned} \tag{5}$$

where α_1 refers to the second-grade fluid material parameter, ρ denotes the fluid density and μ means the dynamic viscosity.

Physical boundary conditions that govern the problem are as follows:

At the middle line symmetry ($\theta = 0$):

$$u = U, \quad \frac{\partial u}{\partial \theta} = 0, \quad \frac{\partial T}{\partial \theta} = 0, \quad \frac{\partial C}{\partial \theta} = 0. \tag{6}$$

At the channel wall ($\theta = \alpha$):

$$\begin{aligned} u =& -L_1\left[\frac{1}{r}\frac{\partial u}{\partial \theta} + \frac{\alpha_1}{\mu}\left(-\frac{2u}{r^3}\frac{\partial u}{\partial \theta} + \frac{\partial^2 u}{\partial r \partial \theta}\left(\frac{u}{r}\right)\right.\right. \\ &\left.\left.+\frac{1}{r}\frac{\partial u}{\partial r}\frac{\partial u}{\partial \theta}\right)\right], \\ T =& T_w - L_2\frac{\partial T}{\partial \theta}, \quad C = C_w - L_3\frac{\partial C}{\partial \theta}. \end{aligned} \tag{7}$$

where, $(\rho c_p)_f$, D_B, D_T represents heat capacity of fluid, Brownian motion coefficient, thermophoresis coefficient respectively.

The radial velocity of the form is well illustrated by the continuity equation, as follows:

$$f(\theta) = ru(r, \theta). \tag{8}$$

Utilizing the above equation into momentum equations (2) and (3), we get

$$\frac{1}{\rho_f}\frac{\partial p}{\partial r} = \frac{1}{r^3}f^2 + \frac{v_f}{r^3}f^4 - \frac{\alpha_1}{\rho_f r^5}\left(8f^2 + 2f^2 + 4ff^4\right). \tag{9}$$

$$\frac{1}{\rho_f}\frac{\partial p}{\partial \theta} = \frac{2v_f}{r^2}f' + 2\frac{\alpha_1}{\rho_f r^4}f'f''. \tag{10}$$

Differentiating Eq. (9) w.r.t "θ" and Eq. (10) w.r.t "r", we get:

$$\frac{1}{\rho_f}\frac{\partial^2 p}{\partial r\partial \theta} = \frac{2}{r^3}ff' + \frac{v_f}{r^3}f''' - \frac{\alpha_1}{\rho_f r^5}\left(16ff' + 4ff'' + 4ff''' + 4f'f''\right). \tag{11}$$

$$\frac{1}{\rho_f}\frac{\partial^2 p}{\partial \theta\partial r} = -4\frac{v_f}{r^3}f' - 8\frac{\alpha_1}{\rho_f r^5}f'f''. \tag{12}$$

Eliminating the pressure term from Eqs. (11) and (12), we arrive at a single flow equation governing the converging/diverging flow of second-grade fluid:

$$\frac{v_f}{r^2}\left(f''' + 4f' + \frac{2}{v_f}ff'\right) - \frac{4\alpha_1}{\rho_f r^4}\left(f'f''' + 4ff'\right) = 0. \tag{13}$$

Dimensionless transformations

The modelled problem is transformed using the following additional transformations to produce its dimensionless form:

$$F(\eta) = \frac{f(\theta)}{rU}, \quad \eta = \frac{\theta}{\alpha}, \quad \beta(\eta) = \frac{T}{T_w}, \quad \varphi(\eta) = \frac{C}{C_w}. \tag{14}$$

Equations for fluid velocity (13), temperature (4), and concentration (5) are changed as follows by applying the subsequent transformation (8) and (14):

$$F''' + 4\alpha^2 F' + 2ReFF' + 4De(FF''' + 4\alpha^2 FF') = 0, \tag{15}$$

$$\beta'' + EcPr\left(4\alpha^2F^2 + F'^2\right) + 2DePrEc\left(FF'^2 + 4\alpha^2F^3\right) + Pr\left(Nt\beta'^2 + Nb\beta'\varphi'\right) = 0, \tag{16}$$

$$\varphi'' + \frac{Nt}{Nb}\beta'' = 0. \tag{17}$$

The above system undergoes the following boundary conditions:

$$F(0) = 1, \quad F'(0) = 0, \quad F(1) + \alpha_1\left(F'(1) + 4DeF(1)F'(1)\right) = 0, \tag{18}$$

$$\beta(1) + \alpha_2\beta'(1) = 1, \quad \beta'(0) = 0, \quad \varphi(1) + \alpha_3\varphi'(1) = 1, \quad \varphi'(0) = 0. \tag{19}$$

where α_1, α_2, α_3 are the velocity, thermal and concentration slip parameters. Here,

$$Pr = \frac{\mu C_p}{k}, \quad Re_r = \frac{r\alpha U}{\nu}, \quad De = \frac{-\alpha_1 U}{r\mu}, \quad Ec = \frac{U^2}{C_p T_w}, \quad \alpha_1 = \frac{L_1 U}{\nu Re}, \quad \alpha_2 = \frac{L_2}{\alpha}, \quad \alpha_3 = \frac{L_3}{\alpha}. \tag{20}$$

3 Emerging Parameters

Skin-friction coefficient and Nusselt number are the physical quantities of interest in this investigation, written as follows:

$$C_f = \left(\frac{\tau_{r\theta}}{\rho U^2}\right)_{\eta=1}, \quad \text{and} \quad Nu = \left(\frac{q_w}{kT_w}\right)_{\eta=1}, \tag{6}$$

where

$$\tau_{r\theta} = \frac{\mu}{r}\frac{\partial u}{\partial \theta} + \alpha_1\left(-\frac{2u}{r^2}\frac{\partial u}{\partial \theta} + \frac{u}{r}\frac{\partial^2 u}{\partial \theta\partial r} + \frac{1}{r}\frac{\partial u}{\partial r}\frac{\partial u}{\partial \theta}\right), \quad q_w = -\frac{k}{r}\frac{\partial T}{\partial \theta}. \tag{21}$$

With the use of similarity transformation, the dimensionless form of Skin friction and Nusselt number are:

$$C_f = \frac{1}{Re}\left(F'(1) + 4DeF(1)F'(1)\right), \quad \text{and} \quad Nu = -\frac{1}{\alpha}\beta'(1), \tag{22}$$

where $Re = \frac{r\alpha U}{\nu}$ signifies the local Reynolds number and the Deborah number $De = \frac{-\alpha_1 U}{\mu r}$.

4 Numerical Method

A powerful and widely used numerical approach for solving boundary value problems (BVPs) involving ordinary differential equations (ODEs) is the finite difference method with a collocation technique. For the purposes of this study, the set of non-linear ODEs governing the flow problem, along with their associated boundary conditions, were solved numerically using the built-in MATLAB function bvp4c. This solver employs a finite difference scheme on an adaptive mesh, which allows for efficient and accurate computation of solutions, particularly for complex, non-linear systems. To facilitate this process, the higher-order non-linear ODEs were first reduced to a system of first-order ODEs by introducing new variables. This transformation is a necessary step for implementation with the bvp4c procedure. The numerical results were then used to analyze the velocity profile, temperature distribution, heat transfer rate, and skin friction coefficient, providing a comprehensive understanding of the influence of velocity, thermal, and solutal slip conditions on the flow fields. To use this technique, higher order non-linear ODEs (15), (16), and (17) as well as the boundary conditions 18 and (19) must be reduced to first order by choosing the appropriate variables.

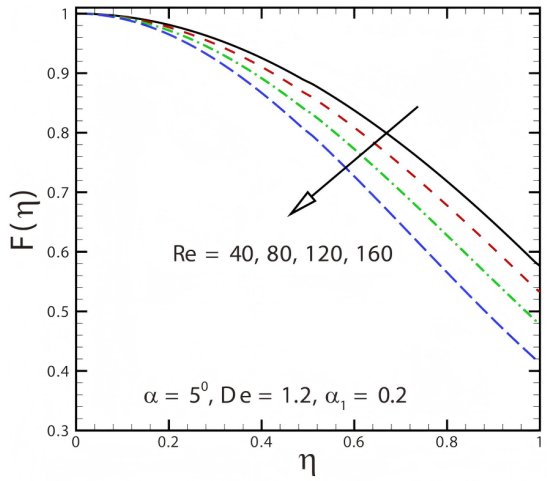

(a): Variation in F(η) for diverging channel with different Re.

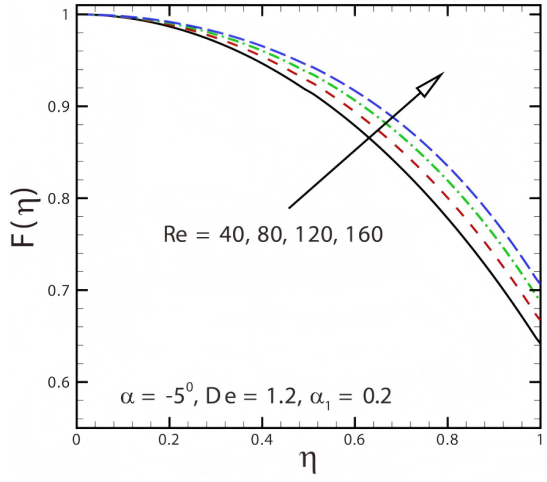

(b): Variation in F(η) for converging channel with different Re.

Figure 2. Variation of velocity profile $F(\eta)$ with Reynolds number Re in (a) diverging and (b) converging channels.

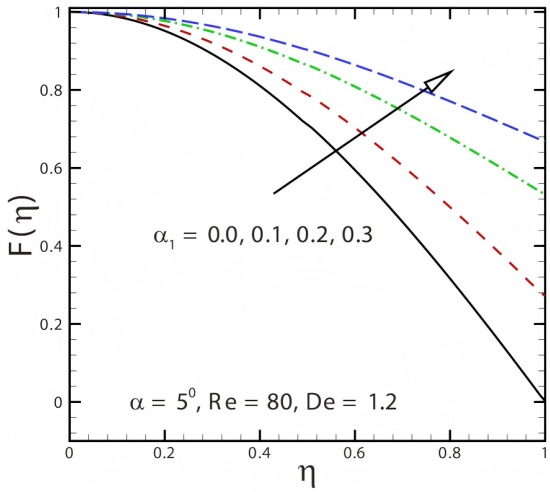

(a): Variation in F(η) for diverging channel with different α_1.

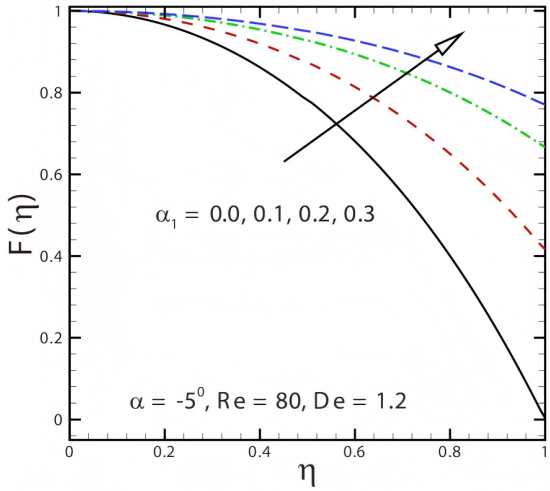

(b): Variation in F(η) for converging channel with different α_1.

Figure 3. Effect of velocity slip parameter α_1 on velocity profile $F(\eta)$ in (a) diverging and (b) converging channels.

Therefore, we introduce the following new variables,

$$
\begin{aligned}
F &= y_1, \\
F' &= y_2, \\
F'' &= y_3, \\
\beta &= y_4, \\
\beta' &= y_5, \\
\varphi &= y_6, \\
\varphi' &= y_7.
\end{aligned}
$$

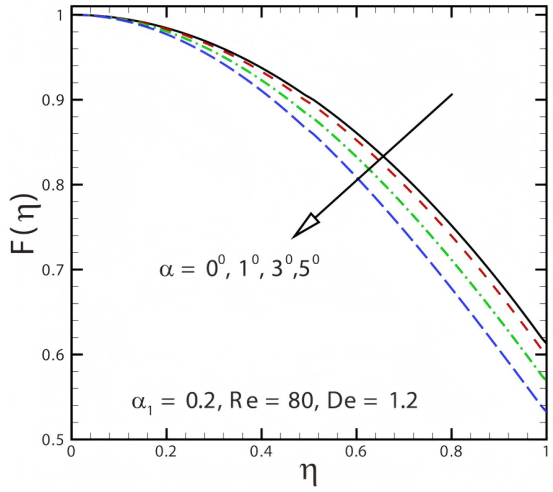

(a): Variation in F(η) for diverging channel with different α.

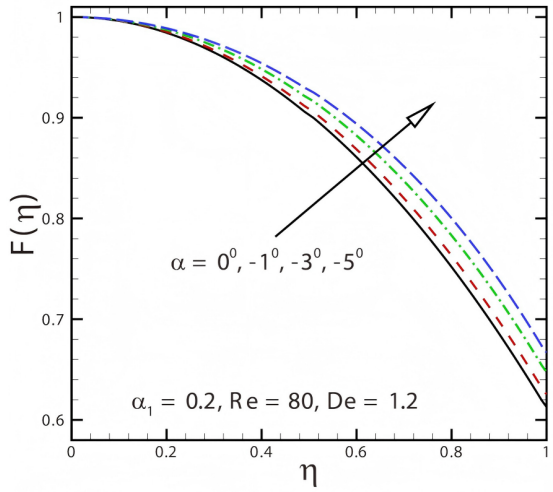

(b): Variation in F(η) for converging channel with different α.

Figure 4. Effect of wall inclination angle α on velocity profile $F(\eta)$ in (a) diverging and (b) converging channels.

Consequently, the obtained set of first order ODEs is:

$$
\begin{aligned}
y_1' &= y_2, \\
y_2' &= y_3, \\
y_3' &= yy_1 = \frac{-4\alpha^2 y_2 - 2\alpha Re y_1 y_2 - 16De \cdot \alpha^2 y_1 y_2}{1 + 4De \cdot y_1}, \\
y_4' &= y_5, \\
y_5' &= yy_2 = -EcPr(4\alpha^2 y_1^2 + y_2^2) \\
&\quad - 2DePrEc(y_1 y_2^2 + 4\alpha^2 y_1^3) \\
&\quad - Pr(Nb \cdot y_7 y_5 + Nt \cdot y_5^2), \\
y_6' &= y_7, \\
y_7' &= \varphi'' = yy_3 = \frac{-Nt}{Nb} yy_2.
\end{aligned}
$$

The boundary conditions become:

$$
\begin{aligned}
&y_1(0) = 1, \\
&y_2(0) = 0, \\
&y_1(1) + \alpha_1[y_2(1) + 4Dey_1(1) \cdot y_2(1)] = 0, \\
&y_5(0) = 0, \\
&y_4(1) + \alpha_2 y_5(1) = 1, \\
&y_7(0) = 0, \\
&y_6(1) + \alpha_3 y_7(1) = 1.
\end{aligned}
$$

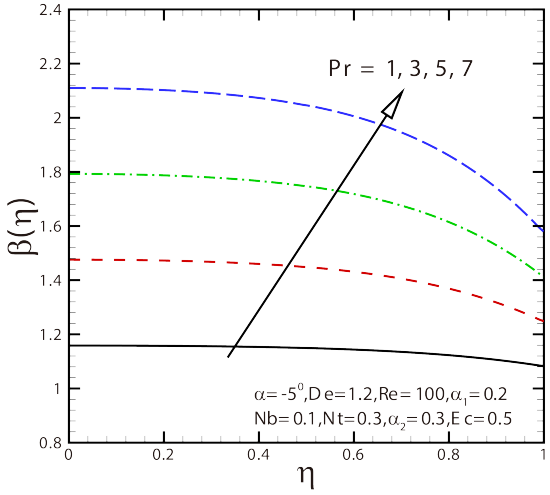

Figure 5. Variation in $\beta(\eta)$ for converging channel with different Pr.

5 Result and discussion

The focus of this section is on how emerging parameters affect velocity, temperature and concentration profiles $F(\eta)$, $\beta(\eta)$ and $\varphi(\eta)$ respectively. In Figures 2–12, the field quantities are plotted against the similarity variable, η, for various values of existing parameters.

The behavior of velocity for different emerging parameters is presented in Figures 2, 3 and 4. Figure 2(a, b) represents the variation in Reynolds

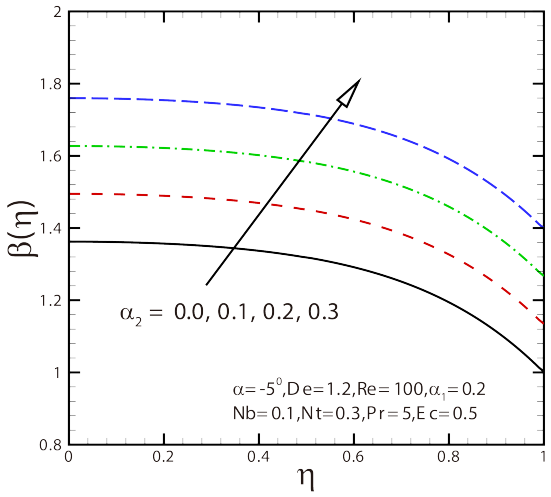

Figure 6. Variation in $\beta(\eta)$ for converging channel with different α_2.

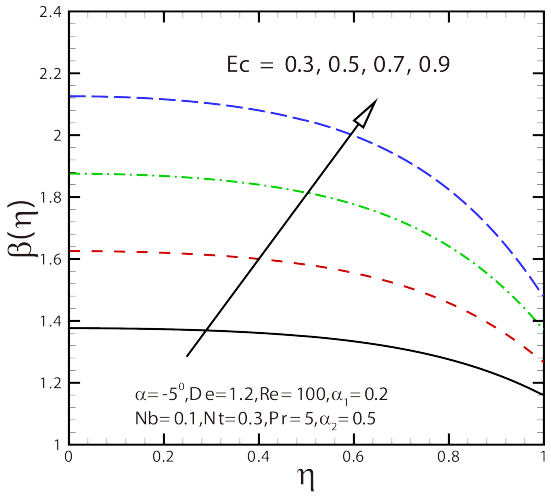

Figure 7. Variation in $\beta(\eta)$ for converging channel with different Ec.

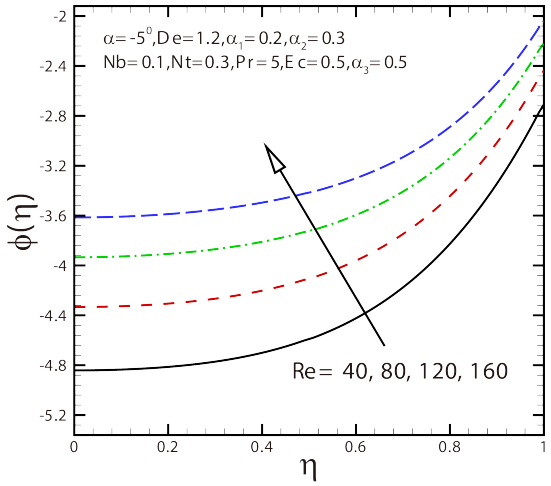

Figure 8. Variation in $\phi(\eta)$ for converging channel with different Re.

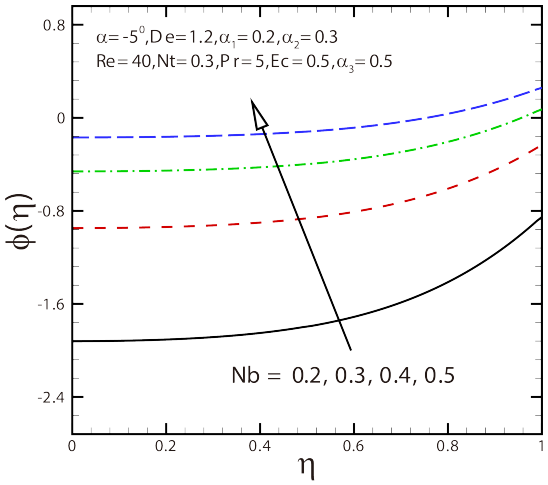

Figure 9. Variation in $\phi(\eta)$ for converging channel with different Nb.

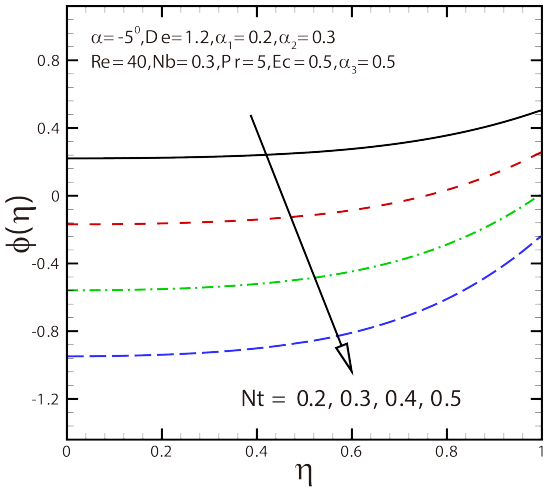

Figure 10. Variation in $\phi(\eta)$ for converging channel with different Nt.

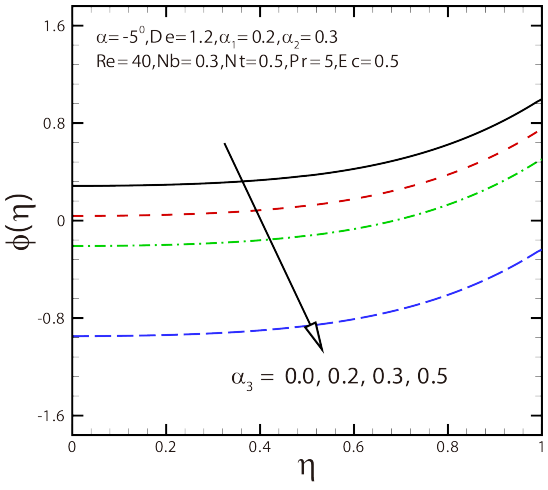

Figure 11. Variation in $\phi(\eta)$ for converging channel with different α_3.

number for converging and diverging channels. One can see that an increase in Reynolds number results in an increase in the velocity $F(\eta)$ in convergent channel while for stretching case, we can observe that with the increase in the Reynolds number, $F(\eta)$ decreases.

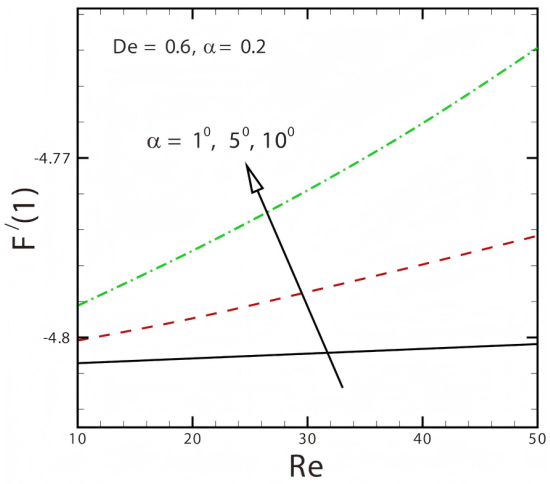

(a): Effect of Re on skin friction for divergent channel.

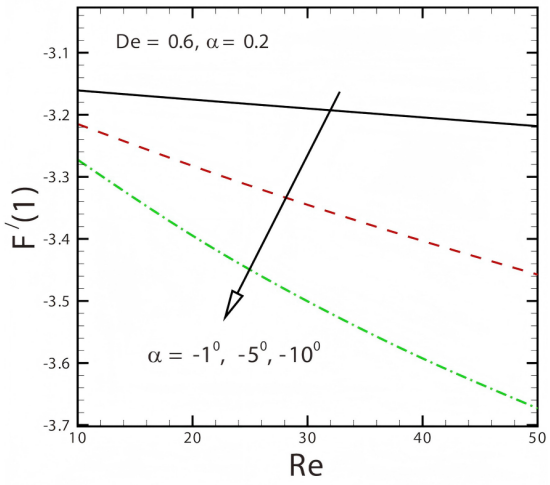

(b): Effect of Re on skin friction for convergent channel.

Figure 12. Effect of Reynolds number Re on skin friction coefficient in (a) divergent and (b) convergent channels.

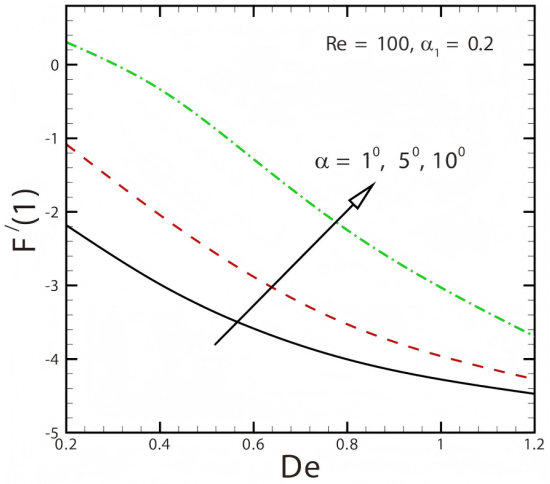

(a): Effect of De on skin friction for divergent channel.

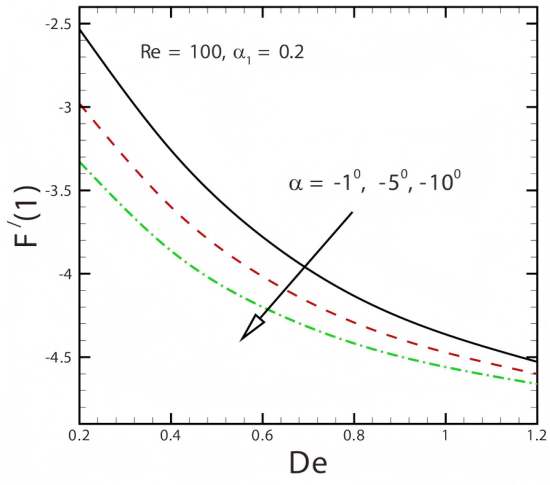

(b): Effect of De on skin friction for convergent channel.

Figure 13. Effect of Deborah number De on skin friction coefficient in (a) divergent and (b) convergent channels.

Figure 3(a, b) makes it evident that in both cases, the velocity $F(\eta)$ increases for increasing values of velocity slip parameter, α_1. It is also investigated how variations in the inclination between the channel walls affect F shown by Figure 4 and it is found that velocity decreases as the inclination between the channel walls of a diverging channel increase. In contrast, $F(\eta)$ rises in a convergent channel as α rises.

In Figure 5, it is possible to see how variation in Pr affect the temperature distribution for both converging and diverging flows. With an increase in Pr in each case, the temperature profile increases. Like this, temperature profile rises with an increase in thermal slip parameter (α_2) and Eckert number (Ec), shown in Figures 6 and 7.

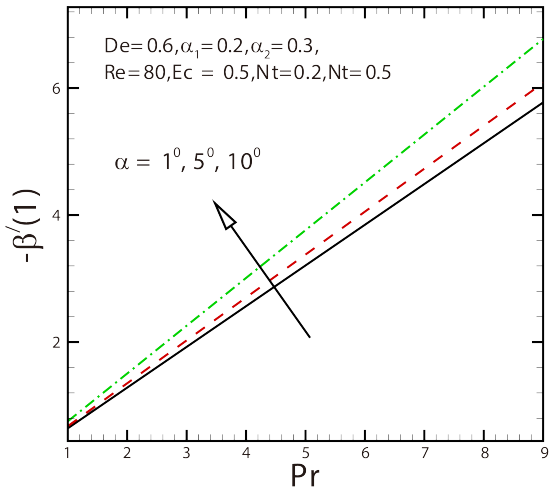

Figure 14. Effect of Pr on Nusselt number for divergent channel.

For various values of Re, Nb, Nt, and α_3, the profiles for mass fraction are graphed in Figures 8, 9, 10 and 11. Figure 8 shows that an increase in the values of the Reynolds number, $\varphi(\eta)$ increases. Figure 9 depicts the effects of Brownian motion on concentration and increasing behavior is found for

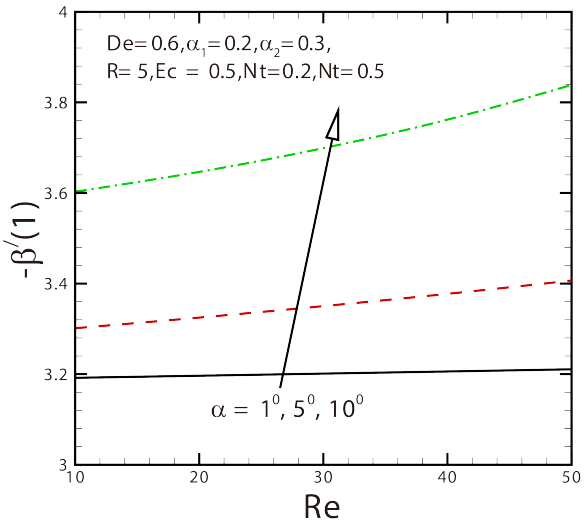

Figure 15. Effect of Pr on Nusselt number for convergent channel.

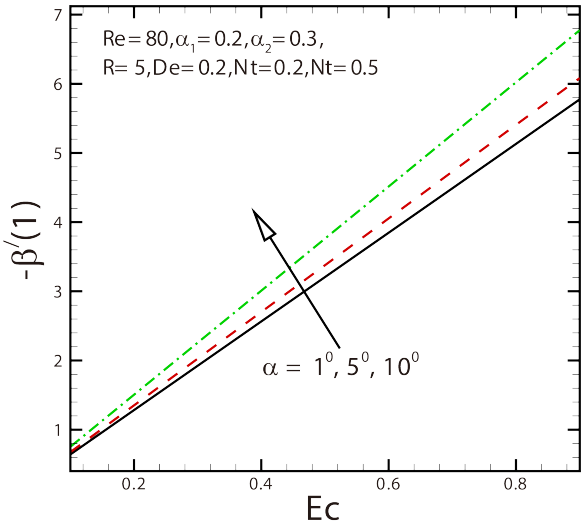

Figure 17. Effect of Ec on Nusselt number for convergent channel.

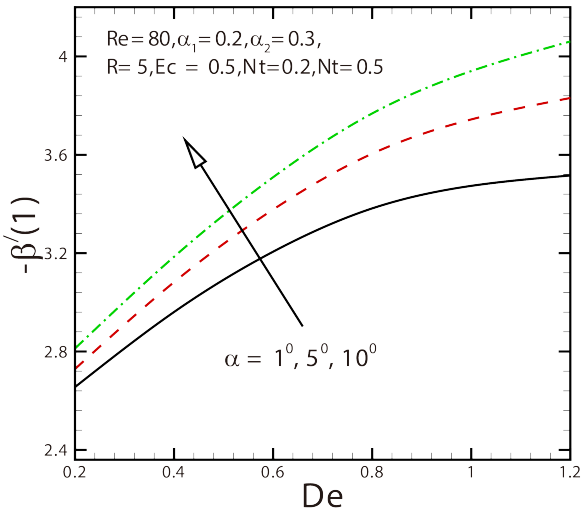

Figure 16. Effect of De on Nusselt number for convergent channel.

both channels. Figure 10 shows the increasing values of the thermophoresis parameter and how they affect concentration and it is noticed that an increase in the value of Nt decreases concentration. Figure 11 shows the increasing values of α_3, decreases concentration. Figures 12 and 13 demonstrate how changes in various parameters affect the skin friction coefficient. The effect of Reynolds number on skin friction is depicted in Figure 12(a, b). The effect of Re on skin friction is reported to be growing for higher values of α while the behavior is seen to be decreasing for $\alpha < 0$. Figure 13(a, b) depicts the influence of Deborah number. As Deborah number rises, skin friction decreases in convergent channel, whereas on divergent channel, the results are opposite. The effects of different factors on Nusselt number are depicted in Figures 14, 15, 16 and 17. Growing behavior is displayed by Prandtl, Reynolds, Deborah and Eckert number on Nusselt number.

6 Conclusion

The study focuses on the observation of multi-slips mechanism to converging and diverging flow of a non-Newtonian fluid with heat transfer on nanofluids. Basic governing equations of flow are reduced into a system of non-linear ODE's which are then translated into PDE's via a similarity transformation. Additionally, a built-in MATLAB code is employed to derive solutions and generate graphs for Nusselt number, skin friction, temperature profile and velocity against different parameters. Hence, following are the major conclusions from our analysis:

1. In both divergent & convergent channels, Re and α have the same effect on the velocity profile; that is, as these parameters are increased, the velocity profile increases in convergent case and decreases in divergent case.
2. The dimensionless temperature $\beta(\eta)$ is an increasing function of Re, De, Pr, Ec in convergent and divergent channel.
3. Increased velocity at the wall is the result of fluid slip at the wall.
4. In convergent and divergent channels, Re and De have the opposite effects on the skin friction coefficient.
5. With respect to both converging and diverging channels, the prandlt number behaves in a way that increases for temperature profiles while

decreases for concentration profiles. The fluid concentration for both channels was improved by the Brownian motion parameter as well.

Data Availability Statement

Data will be made available on request.

Funding

This work was supported without any funding.

Conflicts of Interest

The authors declare no conflicts of interest.

Ethical Approval and Consent to Participate

Not applicable.

References

[1] Choi, S. U. (1995, November). Enhancing thermal conductivity of fluids with nanoparticles. In *ASME international mechanical engineering congress and exposition* (Vol. 17421, pp. 99-105). American Society of Mechanical Engineers. [CrossRef]

[2] Buongiorno, J. (2006). Convective transport in nanofluids. *ASME Journal of Heat Transfer, 128*(3), 240–250. [CrossRef]

[3] Khan, W. A., & Pop, I. (2010). Boundary-layer flow of a nanofluid past a stretching sheet. *International Journal of Heat and Mass Transfer, 53*(11–12), 2477–2483. [CrossRef]

[4] Makinde, O. D., & Aziz, A. (2011). Boundary layer flow of a nanofluid past a stretching sheet with a convective boundary condition. *International Journal of Thermal Sciences, 50*(7), 1326–1332. [CrossRef]

[5] Rahman, M. M., Roşca, A. V., & Pop, I. (2014). Boundary layer flow of a nanofluid past a permeable exponentially shrinking/stretching surface with second order slip using Buongiorno's model. *International Journal of Heat and Mass Transfer, 77*, 1133–1143. [CrossRef]

[6] Hashim, & Khan, M. (2016). A revised model to analyze the heat and mass transfer mechanisms in the flow of Carreau nanofluids. *International Journal of Heat and Mass Transfer, 103*, 291-297. [CrossRef]

[7] Dogonchi, A. S., & Ganji, D. D. (2017). Analytical solution and heat transfer of two-phase nanofluid flow between non-parallel walls considering Joule heating effect. *Powder Technology, 318*, 390–400. [CrossRef]

[8] Turkyilmazoglu, M. (2018). Buongiorno model in a nanofluid filled asymmetric channel fulfilling zero net particle flux at the walls. *International Journal of Heat and Mass Transfer, 126*, 974–979. [CrossRef]

[9] Hayat, T., Muhammad, K., Khan, M. I., & Alsaedi, A. (2019). Theoretical investigation of chemically reactive flow of water-based carbon nanotubes (single-walled and multiple walled) with melting heat transfer. *Pramana, 92*(4), 57. [CrossRef]

[10] Hashim, Hafeez, M., & Chu, Y. M. (2021). Numerical simulation for heat and mass transport analysis for magnetic-nanofluids flow through stretchable convergent/divergent channels. *International Journal of Modern Physics B, 35*(19), 2150198. [CrossRef]

[11] O'Neill, M. E., Ranger, K. B., & Brenner, H. (1986). Slip at the surface of a translating-rotating sphere bisected by a free surface bounding a semi-infinite viscous fluid: Removal of the contact-line singularity. *Physics of Fluids, 29*(4), 913–924. [CrossRef]

[12] Nadeem, S., Hayat, T., Abbasbandy, S., & Ali, M. (2010). Effects of partial slip on a fourth-grade fluid with variable viscosity: An analytic solution. *Nonlinear Analysis: Real World Applications, 11*(2), 856–868. [CrossRef]

[13] Ashmawy, E. A. (2012). Unsteady Couette flow of a micropolar fluid with slip. *Meccanica, 47*(1), 85–94. [CrossRef]

[14] Devakar, M., Sreenivasu, D., & Shankar, B. (2014). Analytical solutions of couple stress fluid flows with slip boundary conditions. *Alexandria Engineering Journal, 53*(3), 723–730. [CrossRef]

[15] Hayat, T., Shafique, M., Tanveer, A., & Alsaedi, A. (2016). Magnetohydrodynamic effects on peristaltic flow of hyperbolic tangent nanofluid with slip conditions and Joule heating in an inclined channel. *International Journal of Heat and Mass Transfer, 102*, 54–63. [CrossRef]

[16] Khan, M., Hashim, & Hafeez, A. (2017). A review on slip-flow and heat transfer performance of nanofluids from a permeable shrinking surface with thermal radiation: Dual solutions. *Chemical Engineering Science, 173*, 1–11. [CrossRef]

[17] Xu, H., & Cui, J. (2018). Mixed convection flow in a channel with slip in a porous medium saturated with a nanofluid containing both nanoparticles and microorganisms. *International Journal of Heat and Mass Transfer, 128*, 1043–1053. [CrossRef]

[18] Turkyilmazoglu, M. (2019). Fully developed slip flow in a concentric annuli via single and dual phase nanofluids models. *Computer Methods and Programs in Biomedicine, 179*, 104997. [CrossRef]

[19] Bilal, M. (2020). Micropolar flow of EMHD nanofluid with nonlinear thermal radiation and slip effects. *Alexandria Engineering Journal, 59*(2), 965–976. [CrossRef]

[20] Bég, O. A., Bég, T., Khan, W. A., & Uddin, M. J. (2021). Multiple slip effects on nanofluid dissipative flow in a converging/diverging channel: A numerical study. *Heat Transfer, 51*(1), 1040–1061. [CrossRef]

[21] Motsa, S. S., Sibanda, P., Awad, F. G., & Shateyi, S.

(2010). A new spectral-homotopy analysis method for the MHD Jeffery–Hamel problem. *Computers & Fluids, 39*(7), 1219–1225. [CrossRef]

[22] Hayat, T., Nawaz, M., & Sajid, M. (2010). Effect of heat transfer on the flow of a second-grade fluid in divergent/convergent channel. *International Journal for Numerical Methods for Fluids, 64*(7), 761–776. [CrossRef]

Dr. Hashim s a distinguished scholar in the field of Applied Mathematics, with a specialized focus on fluid mechanics and heat transfer. He earned his Ph.D. in Applied Mathematics from Quaid-I-Azam University, Islamabad in 2018. (Email: hashim@uoh.edu.pk)